Role of atrial wall thickness in wave-dynamics of atrial fibrillation

Jin Wi

Department of Medicine

The Graduate School, Yonsei University

Role of atrial wall thickness in wave-dynamics of atrial fibrillation

Directed by Professor Hui-Nam Pak

The Doctoral Dissertation
submitted to the Department of Medicine,
the Graduate School of Yonsei University
in partial fulfillment of the requirements for the degree
of Doctor of Philosophy

Jin Wi

December 2016

This certifies that the Doctoral Dissertation of Jin Wi is approved.

Thesis Supervisor: Hui-Nam Pak

Thesis Committee Member: Moon-Hyoung Lee

Thesis Committee Member: Deok Won Kim

Thesis Committee Member: Seil Oh

Thesis Committee Member: Eun Bo Shim

The Graduate School
Yonsei University

December 2016

ACKNOWLEDGEMENTS

This page is exclusively designed to note my gratitude and respect for those who helped me to complete my dissertation. I am deeply indebted to my supervisor Prof. Hui-Nam Pak for his kind help, guidance, support and encouragement throughout my study. This study would not have been possible without his assistance and cooperation. I would like to express my sincere gratitude to my reviewers, Prof. Moon-Hyoung Lee, Deok Won Kim, Seil Oh, and Eun Bo Shim who had the patience and fortitude to read my dissertation and provided constructive criticism to help me defend it. Their guidance not only improved my thesis but also will benefit my future work. I also sincerely thank my colleagues for their assistance on my work and emotional support. Finally, my wife, daughters, and parents are the ones to whom my special gratitude and respect to go. They always play for my side and strengthen my will to achieve my ambition.

Jin Wi

<TABLE OF CONTENTS>

LIST OF FIGURES

LIST OF TABLES

ABSTRACT

Role of atrial wall thickness in wave-dynamics of atrial fibrillation

Jin Wi

Department of Medicine

The Graduate School, Yonsei University

(Directed by Professor Hui-Nam Pak)

Background/Aims: Atrial fibrillation (AF) progression "begets AF" and causes changes in left atrial (LA) structures, indicating that LA structures and AF wave-dynamics are correlated with each other. This study aimed to investigate the relationship between LA wall thickness (LAWT) or LA geometry and AF wave-dynamics.

Methods: We included 27 patients who underwent AF catheter ablation (15 persistent AF [PeAF], 12 paroxysmal AF [PAF]). We measured the LAWT (excluding fat) and LA bumpiness at 25 distinct locations, and the LA endocardial surface bumpiness from pre-procedural heart computed tomography (CT) images by using customized software. We integrated intra-procedural AF electrograms (6 s at 350-500 points), acquired from PeAF patients, with heart CT images, and calculated the spatial distributions of complex fractionated atrial electrogram-cycle length

(CFAE-CL), dominant frequency (DF) and Shannon entropy (ShEn), which reflect AF wave-dynamics.

Results: 1. The LAWT varied widely between patients, locations, and types of AF. The mean LAWT were 2.1 ± 0.6 mm and regional LAWTs varied from 1.9 to 3.1 mm. 2. The LAWT was inversely correlated with the LA volume in PeAF ($r = -0.565$, $p = 0.028$), but not in PAF. 3. The LAWT was positively correlated with LA bumpiness ($r = 0.272$, $p < 0.001$) and ShEn ($r = 0.233$, $p < 0.001$) and negatively correlated with CFAE-CL ($r = -0.107$, $p = 0.038$). 4. In the multiple regression model of AF wave-dynamics, the major independent determinants of DF were LAWT ($\beta = -0.29$, $p < 0.001$) and ShEn ($\beta = 0.74$, $p < 0.001$). ShEn had significant associations with LAWT ($\beta = 0.19$, $p < 0.001$), DF ($\beta = 0.14$, $p < 0.001$), and CFAE-CL ($\beta = -0.01$, $p < 0.001$). CFAE-CL also had significant associations with LAWT ($\beta = 7.49$, $p = 0.032$) and ShEn ($\beta = -74.00$, $p < 0.001$).

Conclusion: The LAWT changes depending on the type of AF, and has significant correlations with the parameters associated with human AF wave-dynamics, electrical wave-break, and rotors.

Key words: atrial fibrillation, wall thickness, bumpiness, wave-dynamics

Role of atrial wall thickness in wave-dynamics of atrial fibrillation

Jin Wi

Department of Medicine
The Graduate School, Yonsei University

(Directed by Professor Hui-Nam Pak)

I. INTRODUCTION

Atrial fibrillation (AF) causes electrical and structural remodeling of the atrium, making it difficult to restore and maintain sinus rhythm.[1, 2] The recurrence and perpetuation of AF can result in the dilatation of the left atrium (LA), which is clinically considered to have a role in structural remodeling events such as fibrosis and hypertrophy.[3, 4] Although the atrial wall is thin, it also has a multi-layer regional difference in terms of the LA wall thickness (LAWT) and a trans-mural difference in conduction and reentry during AF.[5] Alterations in the LA wall also represent structural remodeling in AF with LA dilatation. Animal studies suggested that the presence of interstitial fibrosis was associated with slow conduction and conduction block within the atria, and consequently facilitated the induction of AF by local re-entry. Konings et al. showed that complex fractionated atrial electrograms (CFAEs) were mostly

recorded during AF in areas of slow conduction, functional conduction block, pivot points, and potential transmural reentries in the atria of patients with AF.[6] The mechanism of AF is still unclear; the two major hypotheses are: the focal source hypothesis and the multiple wavelet hypothesis.[7, 8] The focal source hypothesis explains cardiac fibrillation in terms of stable periodic sources (such as mother rotors) that induce wave breakup, whereas the multiple wavelet hypothesis is predicated on the existence of multiple wavelets that may shrink, collide with other wavelets, or create new rotors. Focal self-maintaining sources called rotors have been suggested as a mechanism for AF.[9-11] In this study, we hypothesized that LAWT is associated with AF wave-dynamics and LA geometry. We investigated the relationships between LAWT and LA geometry, and their association with parameters related to AF wave-dynamics.

II. MATERIALS AND METHODS

1. Study population

The present study includes a total of 27 patients with non-valvular AF (15 Persistent AF [PeAF] and 12 paroxysmal AF [PAF]) who underwent radiofrequency catheter ablation (RFCA) for drug-refractory AF from February 2014 to December 2014. All patients maintained optimal anticoagulation levels (target INR 2.0-3.0) before the procedure, and antiarrhythmic drugs were

discontinued for at least five half-lives of each drug and for at least 4 weeks, especially for amiodarone. We used cardiac computed tomography (CT) to visually define the LA anatomy of each patient before RFCA. Twelve patients with PAF were included only for comparisons with patients with PeAF in LAWT measurements on CT. However, analyses of wave-dynamics were not performed because AF electrograms could not be acquired owing to the termination of AF in patients with PAF.

This study protocol was approved by the Institutional Review Board of Severance Hospital, Yonsei University Health System. All patients provided written informed consent.

2. Cardiac CT

Contrast-enhanced cardiac CT was performed with a dual-source CT scanner (Somatom Definition Flash; Siemens Healthcare, Forchheim, Germany) within 2 days before the ablation procedure. Contrast (Iopamiro 370; Bracco, Milan, Italy) was injected into the antecubital vein at a flow rate of 5 mL/s by using a triple-phase method (60-80 mL pure contrast, 30 mL 70%:30% saline-to-contrast mixture, and 20 mL pure saline), and the scan delay time was determined by using the test-bolus technique. Scanning was performed with the following parameters: prospective electrocardiogram (ECG)-gated axial acquisition targeting end-systolic phase by using the absolute delay method,[12] 80-120 kVp with 280-450 mAs, and a 64 x 0.6 mm slice collimation. The

cardiac CT was reconstructed with a slice thickness of 0.75 mm and an increment interval of 0.5 mm.

3. LA volume measurement by using cardiac CT

LA volume was estimated by automatically tracing the LA borders on three-dimensional (3D) LA reconstruction CT images.[13, 14] We used a Hounsfield unit-based endocardial border detection technique with additional manual correction. The LA appendage (LAA) was included; however, pulmonary veins (PVs) at their ostia were excluded for the measurements of LA volume. The LA was separated from the left ventricle by using the mitral valve leaflets as landmarks. The mitral annulus was excluded at the point of insertion of the mitral valve leaflets.

4. LAWT measurement with cardiac CT

CT images were analyzed with Aquaris Intuition software version 4.4.6 (Terarecon, San Francisco, CA, USA). Two radiologists (with 8 and 11 years of experience with cardiac CT), blinded to the clinical and electrophysiological data of patients, independently evaluated the CT images. The image quality of the cardiac CT was classified as good (no or minor artifact, good diagnostic quality), fair (moderate artifacts, acceptable for diagnosis), or poor (severe artifact impairing accurate evaluation). The presence of an irregular heart rhythm on ECG during the acquisition of cardiac CT was evaluated.

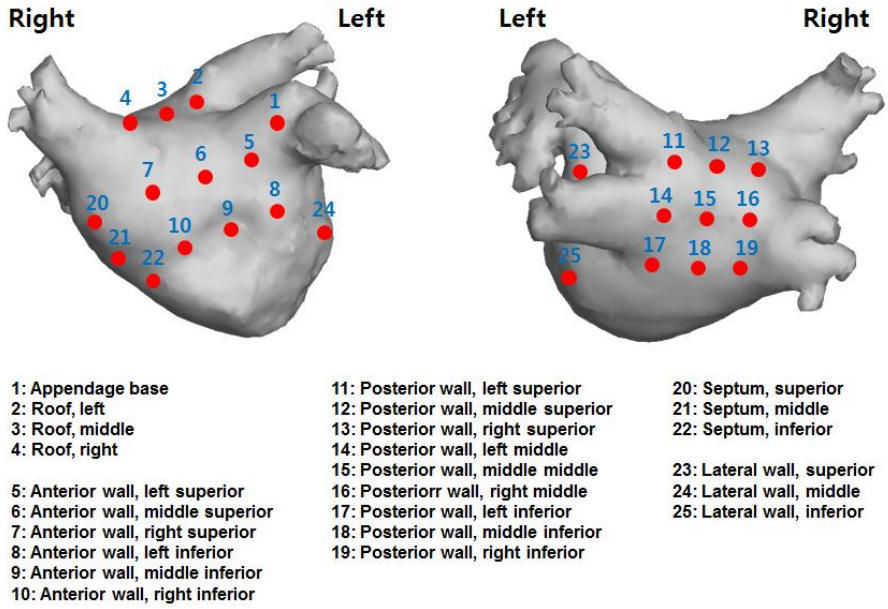

Figure 1. Schematic representation of the 25 preselected left atrial locations. Left panel: anterior view; right panel: posterior view. Lower panel, 25 locations including 3 at the atrial roof, 1 at the anterior appendage base, 6 at the anterior wall, 9 at the posterior wall, 3 at the septum, and 3 at the lateral wall.

All parameters including LAWT were obtained at 25 preselected locations in six regions, including the LAA base, roof, anterior wall, posterior wall, septum, and lateral wall, as suggested by McAlpine, and agreed on between the radiologists and cardiologists (Figure 1).[15] The roof was defined as the most cranial part of the LA, connecting the upper aspect of the venoatrial junctions of the right and left superior PVs. The LAWT of the LAA base was measured at the anterior portion of the LAA neck, within 5 mm of the junction of the LAA

and the LA body. The septum referred to the interatrial muscular wall that separates adjacent atrial chambers. The investigators divided the regions into superior/middle/inferior and left/middle/right portions on the LA surface of the 3D volume-rendered (VR) CT by using the equal virtual grids, and determined a reference point at the center of each portion in every patient. We assessed the wall thickness such that 10 points within 5 mm of each reference point were measured, and calculated the average.

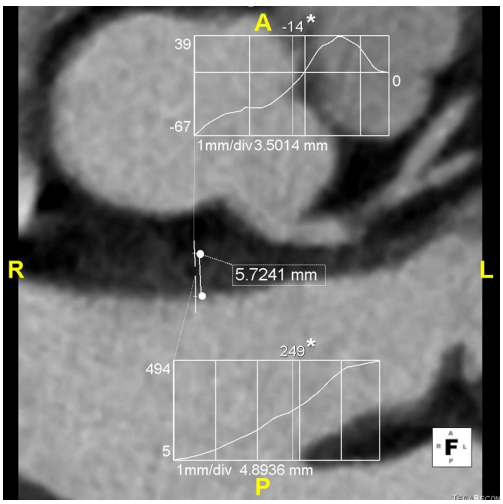

Figure 2. Measurement of left atrial (LA) wall thickness at the middle superior anterior wall. The LA wall thickness was measured semiautomatically between the inner and outer borders through a histogram and a line segment tool by using software. In inset graphs, the numbers in the y-axes denote the extreme computed tomography (CT) numbers of the two short lines across the LA wall and epicardial fat and LA wall and LA cavity. Numbers marked with an asterisk

represent the median CT numbers from the full width at half-maximum method, which correspond with the dots on the line across the LA wall.

The points were determined on the LA surface on the 3D VR, axial, coronal, and sagittal images by using a cross cursor. Thereafter, the observers measured the LAWT on the multiplanar reformatted axial, coronal, and sagittal images to obtain accurate perpendicular measurements, and used semi-automated measurement through a histogram to determine the inner and outer border points of the LA wall correctly (Figure 2). At the preselected point, two short vertical lines across the LA wall and epicardial fat, and across the LA wall and LA cavity were drawn with CT histograms plotting the CT attenuation (the two inset graphs) corresponding to each line. Then, the border points of the LA wall and epicardial fat, and the LA wall and LA cavity were automatically drawn after being derived by using the CT attenuation difference. With this method, the investigators could determine the inner and outer borders of the LA wall at the preselected points. Subsequently, LAWT was automatically measured between the inner and outer margins through a line segment tool available from the used software program.

5. LAWT measurement in cadaver hearts

A postmortem analysis of LAWT was performed in 17 human heart specimens (cadaver hearts), none of which had a history of AF, by using

calipers. We measured the LAWT at 19 preselected locations, including the roof, anterior wall, and posterior wall.

6. Electrophysiological mapping

Intracardiac bipolar electrograms were continuously monitored and recorded by using the Prucka CardioLab Electrophysiology system (General Electric Health Care System Inc., Milwaukee, WI, USA). After obtaining trans-septal access, 3D VR cardiac CT merged 3D electroanatomical mapping (Ensite NavX system; St. Jude Medical Inc., Minneapolis, MN, USA) was performed. By using a multipolar ring catheter (Lasso; Johnson & Johnson Inc., Diamond Bar, CA, USA), the 3D geometry of the LA chamber was reconstructed in real time, and the system recorded the 12-lead ECG at each point. The intracardiac bipolar electrograms were exported at a sampling rate of 2.0 kHz and band-pass filtered from 32 to 300 Hz, thus allowing the electrophysiological information to be color coded and superimposed on the anatomic map.

The electroanatomical mapping points were well-distributed throughout the LA. At each point, 5-s bipolar electrograms, together with the surface ECG, were acquired during AF. Endocardial contact during point acquisition was facilitated by fluoroscopic visualization of catheter motion, with the distance to geometry signaled by the catheter icon on the NavX system. Bipolar electroanatomical data acquired on the NavX system was used in the computer

simulation for the analysis of wave-dynamics.

7. Assessment of AF wave-dynamics

The contact bipolar electrograms acquired from over 350 points on the entire LA endocardial surface in the clinical electrophysiology laboratory were analyzed by using the 3D computer simulation with MATLAB software (MathWorks, Natick, MA, USA). With this, we determined the AF wave-dynamic parameters, including the CFAE-cycle length (CL), dominant frequency (DF), and Shannon entropy (ShEn). These wave-dynamic parameters were measured at 10 points within 5 mm around each of the 25 preselected locations and the mean values were calculated. We merged the CFAE-CL, DF, and ShEn with the 3D LA geometry and created 3D color-coded maps (Figure 3). To generate a CFAE-CL map, we calculated CFAE-CL as the average time duration between consecutive deflections, which were identified by using the downstroke morphology between the local-maximum and the local-minimum amplitudes. CFAEs were defined as those with CL <120 ms.[16] In brief, we used a manually set peak-to-peak sensitivity threshold to exclude baseline noise from the analysis. We set a refractory period of 40 ms to avoid multiple detections of a single deflection event. Furthermore, an electrogram width of 15 ms was set to exclude the detection of the far-field event.[17] We measured the time between discrete deflections in local electrograms over 5 s (based on selectable width and peak-to-peak [>0.03 mV] criteria).

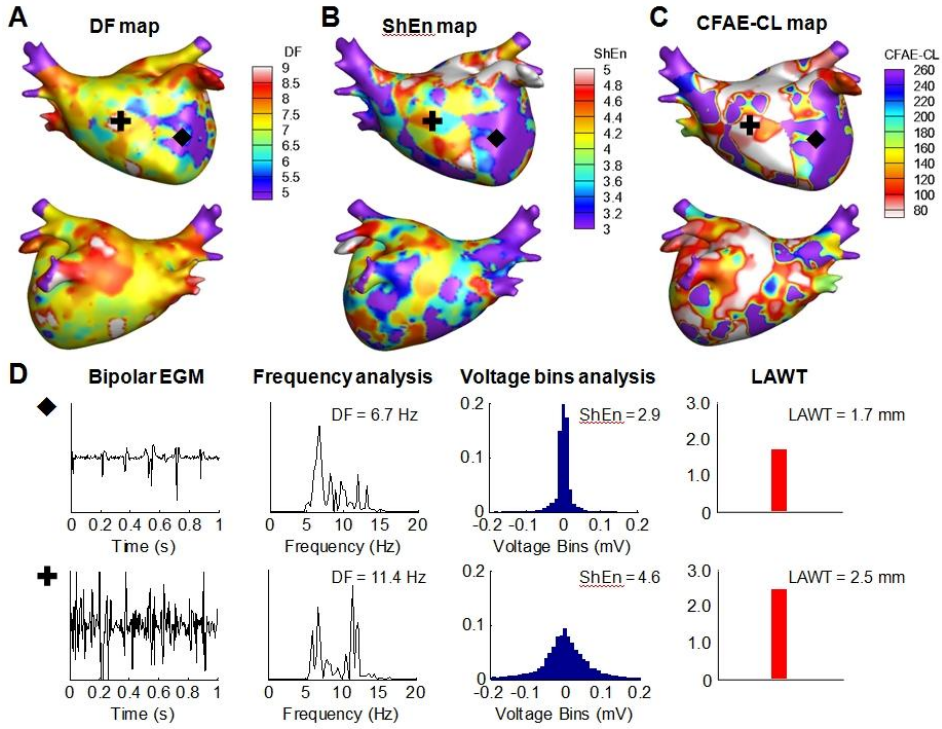

Figure 3. Three-dimensional color-coded AF wave-dynamics maps. (A) DF, (B) ShEn, and (C) CFAE-CL maps. (D) Examples of fractionated and unfractionated EGM and their analyses. The frequency spectrum and voltage histogram were analyzed to compute the DF and ShEn of bipolar EGMs, respectively. Recording sites are marked by black symbols. DF, dominant frequency; ShEn, Shannon entropy; CFAE-CL, complex fractionated atrial electrogram-cycle length; EGM, electrogram; LAWT, left atrial wall thickness.

We performed spectral analysis of the bipolar electrograms to determine the DF.[18] The bipolar signals were tapered at their edges to a 0 value by using the Hanning window, rectified, and band-pass filtered from 3 to 15 Hz, thus

minimizing the double counting of bipolar double potentials <50 ms. An 8192-point fast Fourier transformation with a spectral resolution of 0.24 Hz was performed to obtain the power spectrum of the electrogram at each recording site; in each spectrum, the DF was defined as the frequency with the maximum amplitude at that site for each signal.[19] To ensure reliability in DF detection, we calculated the regularity index (RI), defined as the ratio of the power at the DF and its adjacent frequencies (=0.75-Hz band) to the power of the 3- to 15-Hz band.[20] Points with RI of <0.2 were excluded from the analysis.

The ShEn of the bipolar electrogram was calculated by using the method of Ganesan et al.[21] The voltage histogram of the bipolar signal was generated with 0.01 mV fixed amplitude bins. At each bin, the relative probability density P was calculated by dividing the number of counts in that bin by the total number of counts in all bins. Then, the ShEn was defined as follows:

$$-\sum_{i=0}^{N-1} P_i \log_2 P_i$$

where N is the total number of bins and P_i is the relative probability density of the ith bin.

8. Calculation of the curvature and bumpiness of LA geometry

We reconstructed the LA endocardial geometry from the 3D spiral CT by using the NavX system. The triangular surface mesh of the LA was generated with a spatial resolution of 0.1 cm and HC-Laplacian smoothed to remove the

noise by using MeshLab 1.3.3 software (http://meshlab.sourceforge.net). The LA mesh was uniformly resampled with ACVD software (Creatis, Lyon, France).

At each point of the LA mesh, we calculated the Gaussian curvature (briefly, "curvature") by applying the angle deficit method.[22] To quantize the degree of bumpiness of the nonuniformly curved surface, we defined the surface bumpiness by using the standard deviation (SD) of the curvature as follows:

$$\sqrt{\frac{1}{S}\iint (K-\overline{K})^2\, dA}$$

where S is the surface area, K is the curvature, and $\overline{K}$ is the average of the curvature on the surface. The surface bumpiness represents the heterogeneity of the curvature; that is, how bumpy the tissue is. In the 25 regions of the LA, we calculated the surface bumpiness and the average of the curvature (Figure 4). The C++ code was implemented for the analysis.

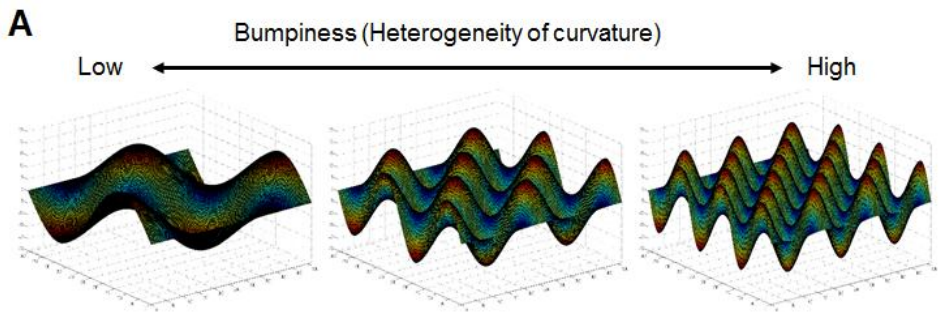

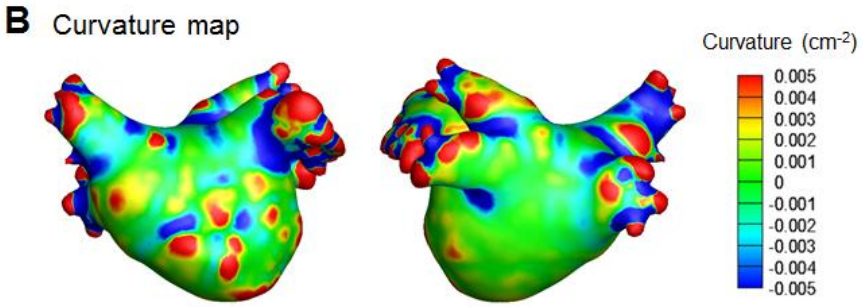

Figure 4. Concepts of curvature and bumpiness. (A) Sites with positive curvature are coded red and sites with negative curvature are coded blue. We defined surface bumpiness to quantize the heterogeneity of curvature. (B) Curvature map of left atrial geometry.

9. Statistical analysis

Continuous variables are expressed as mean ± SD unless otherwise specified. Categorical data are shown as absolute values and percentages. Continuous variables were compared by using Student's t-test or ANOVA. Categorical variables were compared with the $\chi 2$ or Fisher's exact test. Simple and multiple linear regression analyses were performed to determine the relationships between LAWT, LA geometry, and AF wave-dynamics. The degree of association was analyzed by using Pearson's correlation coefficient. To study whether there was an independent relationship between LAWT and AF wave-dynamics, multiple regression analysis was used by forward stepwise selection. We used the intraclass correlation coefficient (ICC) (0-0.20, poor;

0.21-0.40, fair; 0.41-0.60, moderate; 0.61-0.80, good; and 0.81-1.00, excellent agreement) to evaluate the consistency between two observers in the measurements of LAWT. Statistical significance was established at $p < 0.05$, and all statistical analyses were by performed using SPSS version 18.0 (SPSS Inc., Chicago, IL, USA).

III. RESULTS

1. Baseline characteristics

Table 1 shows the baseline clinical characteristics. A total of 27 AF patients (20 men, mean age 60.0 ± 11.1 years, 15 PeAF and 12 PAF) were included in this study. The mean value of CHA_2DS_2-VASc score was 1.9 ± 1.9. The mean left ventricular ejection fraction was 61.7 ± 8.7% and ratio of early diastolic transmitral flow velocity to peak diastolic tissue velocity was 11.0 ± 5.1 on echocardiography. The mean LA volume was 180.1 ± 42.2 mL. Patients with PeAF showed a higher CHA_2DS_2-VASc score (2.5 ± 2.1 vs. 1.2 ± 1.3, p=0.045) and larger LA volume (202.6 ± 37.2 vs. 152.0 ± 30.0 mL, p=0.001) than those with PAF.

Table 1. Baseline characteristics of patients

Variables	Total (n=27)	PeAF (n=15)	PAF (n=12)	p
Male	20 (74%)	11 (73%)	9 (75%)	1.000
Age, years	60.0 ± 11.1	62.3 ± 11.9	57.0 ± 9.7	0.222
65-74	6 (22%)	3 (20%)	3 (25%)	0.756
≥75	2 (7%)	2 (13%)	0 (0%)	0.487
Hypertension	14 (52%)	7 (47%)	7 (58%)	0.547
Diabetes	7 (26%)	5 (33%)	2 (17%)	0.408
Heart failure	0 (0%)	0 (0%)	0 (0%)	-
Stroke	4 (15%)	3 (20%)	1 (8%)	0.605
Vascular disease	4 (15%)	4 (27%)	0 (0%)	0.106
CHA_2DS_2-VASc score	1.9 ± 1.9	2.5 ± 2.1	1.2 ± 1.3	0.045
LA volume, mL	180.1 ± 42.2	202.6 ± 37.2	152.0 ± 30.0	0.001
LVEF, %	61.7 ± 8.7	60.8 ± 10.2	62.8 ± 6.5	0.572
E/E' ratio	11.0 ± 5.1	12.0 ± 6.2	9.7 ± 2.8	0.232

PeAF, persistent atrial fibrillation; PAF, paroxysmal atrial fibrillation; LA, left atrium; LVEF, left ventricular ejection fraction.

2. Regional variability of LAWT

The measurements of LAWT by using CT attenuation differences showed excellent agreement between two independent observers (ICC = 0.979, p <0.001). However, the conventional direct measurements of LAWT through visual assessment demonstrated poorer inter-observer agreement (ICC = 0.791, p <0.001). There was a large inter-patient variation in LAWT, ranging from 1.59 to 2.65 mm. The differences in the mean LAWT in the 25 predefined

anatomic locations are shown in Table 2. The average LAWT was 2.10 ± 0.60 mm and ranged largely from 1.15 to 5.17 mm. Significant differences in LAWT were observed among the 25 locations. The LAA base was found to be the thickest zone (3.13 ± 0.74 mm). The anterior wall such as the middle inferior (2.62 ± 0.73 mm), middle superior (2.57 ± 0.80 mm), and left inferior (2.55 ± 0.86 mm) anterior walls was also thicker than the other areas. On the other hand, the posterior wall, including the right inferior (1.73 ± 0.50 mm), right middle (1.75 ± 0.28 mm), right superior (1.78 ± 0.36 mm), and left superior (1.78 ± 0.29 mm) posterior walls, was found to be the thinnest region.

Table 2. Average LAWT according to location

	Location	Mean LAWT	Range
LAA base	1	3.13 ± 0.74	2.31-5.17
Roof	2	2.08 ± 0.43	1.15-2.88
	3	2.52 ± 0.78	1.56-3.98
	4	1.91 ± 0.33	1.31-2.67
Anterior wall	5	2.22 ± 0.53	1.29-3.16
	6	2.57 ± 0.80	1.49-4.15
	7	1.97 ± 0.64	1.35-3.90
	8	2.55 ± 0.86	1.17-4.65
	9	2.62 ± 0.73	1.69-3.83
	10	2.13 ± 0.53	1.44-3.33
Posterior wall	11	1.78 ± 0.29	1.23-2.21
	12	1.91 ± 0.36	1.33-2.53

	13	1.78 ± 0.36	1.36-2.89
	14	1.83 ± 0.32	1.29-2.52
	15	1.95 ± 0.46	1.43-3.10
	16	1.75 ± 0.28	1.38-2.23
	17	1.97 ± 0.54	1.29-3.60
	18	2.01 ± 0.42	1.56-3.02
	19	1.73 ± 0.50	1.39-2.65
Septum	20	1.89 ± 0.29	1.37-2.35
	21	1.95 ± 0.32	1.35-2.54
	22	1.92 ± 0.31	1.34-2.38
Lateral wall	23	2.14 ± 0.52	1.35-3.58
	24	2.09 ± 0.45	1.37-2.77
	25	2.10 ± 0.60	1.36-2.51

LAWT, left atrial wall thickness; LAA, left atrial appendage.

Values are expressed as mm.

There was a significant regional variability in LAWT, including other parameters (Table 3). The LAA base had the thickest wall and the posterior wall was the thinnest (3.13 ± 0.74 vs. 1.86 ± 0.40 mm, $p<0.001$). The anterior wall (2.34 ± 0.72 mm) and roof (2.17 ± 0.59 mm) were thicker than the mean LAWT, whereas the septum (1.92 ± 0.30 mm) and lateral wall (2.08 ± 0.43 mm) were thinner. In addition, we observed that the LAWT was inversely associated with the LA volume (Figure 5). However, an inverse relation between LAWT and LA volume was found in patients with PeAF, but not in those with PAF.

Table 3. Comparisons of parameters according to the LA regions

	Total (N=375)	LAA base (n=15)	Roof (n=45)	Anterior wall (n=90)	Posterior wall (n=135)	Septum (n=45)	Lateral wall (n=45)	p
LAWT, mm	2.10±0.60	3.13±0.74	2.17±0.59	2.34±0.72	1.86±0.40	1.92±0.30	2.08±0.43	<0.001
DF, Hz	6.76±0.95	6.92±1.24	6.79±0.95	6.61±0.93	6.92±0.99	6.57±0.81	6.73±0.89	0.147
ShEn	4.00±0.64	4.63±0.72	3.98±0.66	3.93±0.65	3.99±0.57	3.86±0.65	4.14±0.63	0.001
CFAE-CL, ms	151.75± 60.54	129.95± 45.33	159.45± 67.14	153.87± 62.37	145.44± 53.77	150.85± 60.71	166.88± 70.98	0.215
CFAE, n	136 (36%)	8 (53%)	12 (27%)	30 (33%)	57 (42%)	15 (33%)	14 (31%)	0.238
Curvature	-0.05±0.20	-0.37±0.47	-0.18±0.19	-0.02±0.12	-0.06±0.16	0.04±0.08	0.05±0.18	<0.001
Bumpiness	0.31±0.38	1.72±0.33	0.36±0.23	0.23±0.19	0.20±0.22	0.20±0.13	0.36±0.37	<0.001

LA, left atrium/left atrial; LAA, left atrial appendage; LAWT, left atrial wall thickness; CFAE, complex fractionated atrial electrograms; CL, cycle length; DF, dominant frequency; ShEn, Shannon entropy.

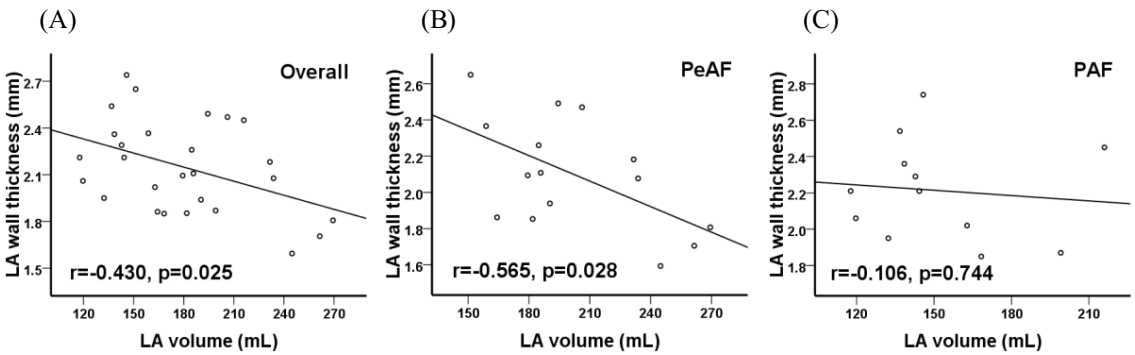

Figure 5. Relationship between LA wall thickness and LA volume. The LA wall thickness was inversely associated with LA volume in AF (A). An inverse relation was also observed in PeAF (B), but not in PAF (C). LA, left atrial; AF,

atrial fibrillation; PeAF, persistent atrial fibrillation; PAF, paroxysmal atrial fibrillation.

An analysis of the LAWT by using calipers in structurally normal cadaver heart specimens also showed significant regional differences in LAWT with an average thickness of 1.5 ± 0.9 mm (Table 4). There was a similar tendency in terms of regional differences of LAWT in AF hearts of patients and in cadaver heart specimens. While the anterior wall was the thickest, the posterior wall was the thinnest in cadaver specimens (2.13 ± 0.61 vs. 1.15 ± 0.84 mm, p <0.001).

Table 4. Comparisons of LAWT between AF hearts and 19 human cadaver heart specimens

	Roof	Anterior wall	Posterior wall	p
AF	2.17 ± 0.59	2.34 ± 0.72	1.86 ± 0.40	<0.001
Cadaver	1.89 ± 0.90	2.13 ± 0.61	1.15 ± 0.84	<0.001

AF, atrial fibrillation.

Values are expressed as mm.

Table 5 shows the comparisons of regional LAWTs according to types of AF. The mean LAWT in PeAF was thinner than in PAF (2.10 ± 0.60 vs. 2.21 ± 0.91 mm, p = 0.049). There were regional differences in LAWT between PeAF and PAF. Whereas the roof (2.17 ± 0.59 vs. 2.94 ± 0.81 mm, p <0.001) and the posterior wall (1.86 ± 0.40 vs. 2.14 ± 0.63 mm, p <0.001) were significantly

thinner, the lateral wall (2.08 ± 0.43 vs. 1.39 ± 0.40 mm, p <0.001) was thicker in PeAF than in PAF. In PAF, the LAA base was the thickest, whereas the lateral wall was the thinnest (3.25 ± 2.36 vs. 1.39 ± 0.40 mm, p <0.001).

Table 5. Comparisons of LAWT according to types of AF

	PeAF (n=15)	PAF (n=12)	p
LAA base	3.13 ± 0.74	3.25 ± 2.36	0.790
Roof	2.17 ± 0.59	2.94 ± 0.81	<0.001
Anterior wall	2.34 ± 0.72	2.42 ± 1.00	0.562
Posterior wall	1.86 ± 0.40	2.14 ± 0.63	<0.001
Septum	1.92 ± 0.30	1.77 ± 0.73	0.241
Lateral wall	2.08 ± 0.43	1.39 ± 0.40	<0.001
Overall	2.10 ± 0.60	2.21 ± 0.91	0.049

PeAF, persistent atrial fibrillation; PAF, paroxysmal atrial fibrillation; LAA, left atrial appendage.

Values are expressed as mm.

3. Regional variability of LA geometry and AF wave-dynamics

We analyzed wave-dynamics of 15 PeAF patients whose electrograms were acquired during AF. AF electrograms taken from 350-500 points were integrated to the geometry of the LA-CT image, calculated CFAE-CL, DF, ShEn, and displayed color-coded color maps by using the customized software we developed. We observed a large inter-patient variation in AF wave-dynamics

and LA geometry as follows: CFAE-CL 151.75 ± 31.90 ms (range, 94.92-203.24 ms), DF 6.76 ± 0.85 Hz (range, 5.61-8.40 Hz), ShEn 4.00 ± 0.43 (range, 3.41-4.98), curvature -0.053 ± 0.030 (range, -0.116-0.026), and bumpiness 0.306 ± 0.078 (range, 0.175-0.476).

Among the LA geometry and AF wave-dynamic parameters, ShEn, curvature, and bumpiness also showed regional differences (Table 3). The LAA base had the highest value of ShEn and the septum had the lowest (4.63 ± 0.72 vs. 3.86 ± 0.65 mm, $p < 0.001$). In the curvature, the highest regional difference between the LAA base and the lateral wall (-0.37 ± 0.47 vs. 0.05 ± 0.18, $p < 0.001$) was observed. The largest regional difference in bumpiness was found between the LAA base and the septum (1.72 ± 0.33 vs. 0.20 ± 0.13, $p < 0.001$).

4. Relationship of LAWT and parameters representing AF wave-dynamics or LA geometry

Table 3 showed that the LAA base, the thickest region, had the shortest CFAE-CL and the highest prevalence of DF, ShEn, and CFAE, compared with the other LA regions. There is also an example showing the relationship between LAWT and AF wave-dynamics. In Figure 3, the right superior anterior wall ("+") demonstrated shorter CFAE-CL (83.5 vs. 158.4 ms) and higher DF (11.4 vs. 6.7 Hz) and ShEn (4.6 vs. 2.9) than the left inferior anterior wall ("◆"). In this patient, the LA wall was significantly thicker at the right inferior anterior wall than at the left inferior anterior wall (2.5 vs. 1.7 mm).

Figure 6 shows the relationship of LAWT to the AF wave-dynamics and LA geometry. In univariate linear regression analyses, LAWT was positively correlated with LA bumpiness ($r = 0.272$, $p < 0.001$) and ShEn ($r = 0.233$, $p < 0.001$) and negatively correlated with CFAE-CL ($r = -0.107$, $p = 0.038$). Furthermore, LA bumpiness also had spatial correlations with ShEn ($r = 0.115$, $p = 0.026$). Additionally, among the parameters of AF wave-dynamics, DF showed a positive correlation with ShEn ($r = 0.454$, $p < 0.001$) and a negative correlation with CFAE-CL ($r = -0.380$, $p < 0.001$). A significant negative association between ShEn and CFAE-CL was observed ($r = -0.760$, $p < 0.001$). In LA geometry, we observed a statistically significant inverse correlation between bumpiness and curvature ($r = -0.498$, $p < 0.001$)

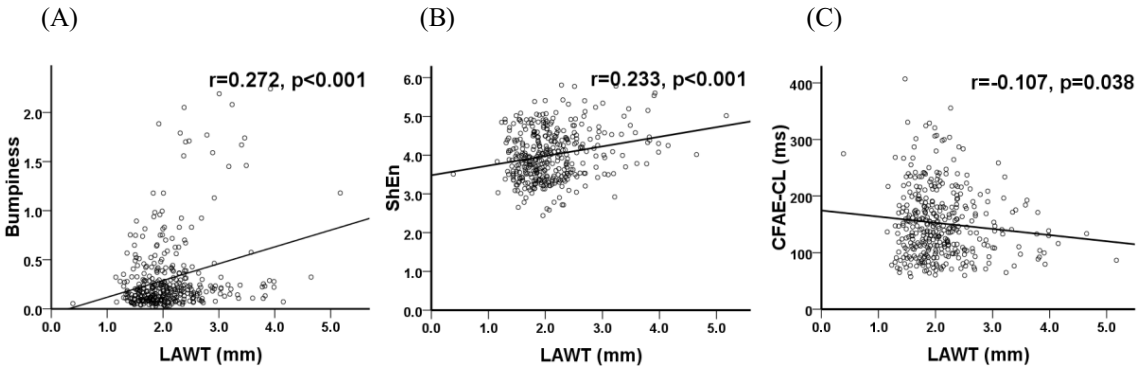

Figure 6. Relationships of LAWT to LA geometry and AF wave-dynamics. (A) LAWT and bumpiness; (B) LAWT and ShEn; (C) LAWT and CFAE-CL. LAWT, left atrial wall thickness; ShEn, Shannon entropy; CFAE-CL, complex fractionated atrial electrogram-cycle length.

To determine whether the LAWT and AF wave-dynamic parameters influence the other parameters of wave-dynamics, stepwise multiple regression models were constructed for each wave-dynamic parameter (Table 6). DF was independently and negatively associated with LAWT (β=-0.29, p<0.001) and positively correlated with ShEn (β = 0.74, p <0.001). ShEn was positively associated with LAWT (β = 0.19, p <0.001) and DF (β = 0.14, p <0.001), but negatively associated with CFAE-CL (β = -0.01, p <0.001). CFAE-CL also showed a positive association with LAWT (β = 7.49, p = 0.032) but a negative association with ShEn (β = -74.00, p <0.001).

Table 6. Stepwise linear regression analyses for the parameters representing AF wave-dynamics

	Univariate			Multivariate		
	β	95% CI	p	β	95% CI	p
DF						
LAWT	-0.10	-0.27~0.06	0.206	-0.29	-0.44~-0.14	<0.001
ShEn	0.68	0.54~0.82	<0.001	0.74	0.61~0.88	<0.001
CFAE-CL	-0.01	-0.01~-0.00	<0.001			
ShEn						
LAWT	0.25	0.14~0.35	<0.001	0.19	0.12~0.25	<0.001
DF	0.30	0.24~0.36	<0.001	0.14	0.10~0.19	<0.001

CFAE-CL	-0.01	-0.01~-0.01	<0.001	-0.01	-0.01~-0.01	<0.001
CFAE-CL						
LAWT	-10.86	-21.11~-0.62	0.038	7.49	0.65~14.34	0.032
ShEn	-72.36	-78.65~-66.07	<0.001	-74.00	-80.44~-67.56	<0.001
DF	-24.11	-30.09~-18.13	<0.001			

DF, dominant frequency; LAWT, left atrial wall thickness; ShEn, Shannon entropy; CFAE-CL, complex fractionated atrial electrogram-cycle length.

We also observed a regional discrepancy in the correlations of LAWT with wave-dynamics and LA geometry (Table 7). For example, LAWT was well correlated with wave-dynamic parameters, including CFAE-CL and ShEn, in the anterior wall with a thicker LAWT, but not in the posterior wall with the thinnest LAWT.

Table 7. Regional difference of the correlations among LAWT, LA geometry, and AF wave-dynamics

	DF	ShEn	CFAE-CL	Curvature	Bumpiness
LAA base					
LAWT	r=-0.333 p=0.226	r=0.355 p=0.194	r=-0.394 p=0.146	r=0.264 p=0.341	r=-0.284 p=0.305
Roof					
LAWT	r=0.108 p=0.479	r=0.278 p=0.065	r=-0.183 p=0.229	r=0.120 p=0.433	r=-0.177 p=0.246

Anterior wall					
LAWT	r=0.052 p=0.628	**r=0.287** **p=0.006**	**r=-0.286** **p=0.006**	r=0.165 p=0.121	r=-0.043 p=0.690
Posterior wall					
LAWT	r=-0.127 p=0.142	r=0.079 p=0.360	r=0.042 p=0.630	r=0.132 p=0.126	r=-0.061 p=0.484
Septum					
LAWT	r=-0.085 p=0.579	r=-0.081 p=0.599	r=0.095 p=0.534	r=-0.080 p=0.602	r=0.182 p=0.232
Lateral wall					
LAWT	r=-0.206 p=0.175	r=0.209 p=0.168	r=0.042 p=0.782	**r=-0.328** **p=0.028**	r=0.163 p=0.286

DF, dominant frequency; ShEn, Shannon entropy; CFAE-CL, complex fractionated atrial electrogram-cycle length; LAA, left atrial appendage; LAWT, left atrial wall thickness.

IV. DISCUSSION

1. Main findings

In the present study, we investigated the role of LAWT in human AF wave-dynamics and LA geometry across points over the entire LA. We measured LAWT with the more accurate method of using CT attenuation differences compared to conventional direct measurements by means of visual assessment on CT. LA geometry such as the curvature and bumpiness was calculated by means of computer simulation. The AF wave-dynamic parameters,

including DF, ShEn, and CFAE-CL, were also determined with over 350 points of real contact bipolar electrograms acquired in the clinical electrophysiology laboratory by using specially designed customized software. To our knowledge, this is the first study to demonstrate the relationship between LAWT and LA geometry, and their association with AF wave-dynamics. The first major finding is that the range of LAWT varied, and significant inter-patient and intra-patient regional variabilities in LA geometry and AF wave-dynamic parameters, as well as in LAWT, were observed. There were also regional differences in LAWT according to types of AF (PeAF and PAF). Second, the LAWT was inversely associated with the LA volume in PeAF, but not in PAF. Third, LAWT was correlated with wave-dynamic parameters and LA geometry, and the major independent determinant of AF wave-dynamic parameters in the multiple regression model.

2. Role of LAWT and LA geometry in AF

LA remodeling process includes structural changes such as LA chamber dilation and fibrosis, as well as changes in LA geometry and function. Some investigators suggested a role of LA geometrical changes in AF.[23, 24] Bisbal et al. demonstrated that LA geometry was associated with a history of thromboembolic events and improved risk prediction of thromboembolic events in patients with AF.[24] In addition, LA geometrical remodeling was related to a higher incidence of non-PV foci AF and to AF inducibility and recurrence after

AF ablation.[25, 26] Therefore, these studies suggest that LA geometrical changes were associated with AF susceptibility and increased risk of thromboembolic events in AF.[27, 28]

LA remodeling in AF has been pathologically attributed to interstitial fibrosis, hypertrophied atrial myocytes, and inflammation, leading to changes in LAWT. These pathologic changes could affect the LA and PV structures. A recent study demonstrated that thickened walls of the LA and PV-LA junction were associated with increased bipolar voltage amplitude and ATP-provoked dormant PV conduction.[29] These findings may help in understanding the etiology of AF and can, in part, explain the mechanism of the dormant PV conduction in AF ablation.

3. Role of LAWT in wave-dynamics according to AF progression

In the present study, the LA wall was found to have non-uniform thickness, with a significant regional difference. The LAA base and anterior wall were thicker than other areas, whereas the posterior wall was the thinnest, consistent with a prior study involving the conventional LAWT measurements in patients with PeAF.[30] However, there is a discrepancy in the regional variability of LAWT between some earlier studies and our study. This discrepancy may be due to the mixed population of patients with PAF and normal sinus rhythm (NSR) as well as PeAF. A long duration of AF results in progressive remodeling of the LA and different aspects of regional variability in LAWT,

which were also observed between PeAF and PAF in this study.[31, 32] Furthermore, the human heart specimens used in these studies were preserved in formalin solution, which might have influenced the LAWT, and may not exactly represent the dimensions of the structures *in situ*.

Localized sources of activity, so-called rotors, have been considered a significant mechanism for AF initiation and maintenance.[9, 20] As the focal source hypothesis suggests the existence of spatiotemporally stable sources that induce and maintain fibrillation waves through wave breakup, the rotor has been identified as the target site of ablation. Localized short CL reentry or focal high-frequency activity was observed in sites assumed to harbor rotors. DF and ShEn are AF wave-dynamic parameters that are objective, mechanistically based tools that can assist in mapping locally stable rotors.[18, 21] The mechanisms of CFAE include wavebreak, fibrillatory conduction, rotors, anisotropy or summation of electrograms from overlapping layers of myocardial fibers, autonomic nerves, and simply transient pivoting or wave front collision. Wavebreak and fibrillatory conduction typically occur in close proximity to the core of a rotor, giving rise to CFAEs.[33, 34] The present study also revealed close relationships among AF wave-dynamic parameters such as DF, ShEn, and CFAE, consistent with the results of previous studies.[21, 33]

Meanwhile, AF progression leads to electroanatomical remodeling, which can alter the wave-dynamics, LA wall structure and thickness, and, by extension, the dimensions of the atrium itself.[35-37] Nakamura et al. demonstrated that the

LA wall was significantly thicker in PAF than in either PeAF or NSR, and thicker in PeAF than in NSR. This may indicate that LA structural remodeling accompanies LA wall thickening; however, the LA wall becomes thinner again owing to predominant fibrosis in "excessively progressed" remodeling. The present study showed that the LAWT was inversely associated with the LA volume in PeAF, but not in PAF. In addition, the LA wall was significantly thinner in PeAF than in PAF, especially the posterior wall and roof. Therefore, we may suppose that LA structural remodeling is excessively advanced in those areas which have the thin wall and relatively little contact with other structures according to Laplace's law with AF progression.

Electroanatomical remodeling means that the AF wave-dynamics and the LA structures interact with each other. Remodeling of the LA wall structure and thickness includes proliferation of smooth muscle cells, collagen deposition, and fibrosis, which are associated with slow conduction and conduction block within the atria and consequently facilitate the induction of AF by local re-entry. Konings et al. showed that CFAEs were mostly recorded during AF in LA areas of slow conduction, functional conduction block, and pivot points.[6] The present study revealed that LAWT was associated with wave-dynamic parameters in both simple correlation and multiple regression analyses. Additionally, LAWT was relatively well correlated with wave-dynamic parameters in the anterior wall with a thicker LA wall, but not in the thinnest posterior wall. The proportion of areas with CFAE was smaller in patients with long-lasting AF

who have a more electroanatomically remodeled LA than in those with a less remodeled LA.[38] Accordingly, these findings from our study and previous studies provide a clue about the relationship between LAWT and AF wave-dynamics. AF wave-dynamic parameters may be related to LAWT in thicker regions with an intermediate degree of electroanatomical remodeling in the LA, but not in thin regions with excessively progressed remodeling.

4. Role of imaging in the treatment of cardiac arrhythmias

In the present study, we used the CT attenuation difference for accurate LAWT measurements. The LA wall is a very thin structure, and the inner and outer boundaries of the LA wall in contact with the LA cavity and epicardial fat, respectively, are indistinct. As a result, conventional direct measurements by means of visual assessment on CT might be inaccurate. By using the semi-automated method to distinguish the pure LA wall from adjacent structures, we found the margins of the LA wall and measured LAWT accurately. Furthermore, our method showed excellent reproducibility in LAWT measurements, with much better agreement between two independent observers than the conventional measurement through visual assessment. In addition, we obtained CT-merged 3D electroanatomical mapping with the intracardiac electrograms and CT. Data acquired in the clinical setting were analyzed by using the computer simulation.

The importance of imaging modalities in the treatment of cardiac

arrhythmias is rapidly growing. Cardiac imaging has played a crucial role in showing cardiac structures and characterizing the arrhythmic substrates, especially for the invasive treatment of arrhythmias with more complex substrates such as AF and ventricular tachycardia. Image-guided intervention can also assist in the selection of patients suitable for ablation and in assessing the outcome of the procedure. Recently, besides fluoroscopy, echocardiography, and CT, magnetic resonance imaging (MRI) has shown the ability to provide crucial information in the setting of ablation of complex substrates, including MRI-guided ventricular tachycardia ablation.[39] Additionally, virtual interventions with computer simulations are increasing.[40]

5. Clinical implications

AF progression leads to electroanatomical remodeling, which includes the alteration of AF wave-dynamics, LA wall structure, and LA geometry. This study revealed the relationships among LAWT, AF wave-dynamics, and LA geometry, and showed regional differences in these relationships by using computer simulation of clinical data. These findings may help in understanding electroanatomical remodeling in AF progression.[41] Additionally, this study may provide some potential information in determining the appropriate AF ablation strategy.[40, 42, 43] Performing circumferential PV isolations or additional ablation after PV isolation may be considered in LA regions with a thick wall because these regions may have a higher incidence of dormant PV conduction or

non-PV foci with AF inducibility. Lower radiofrequency energy and shorter contact time may be also appropriate for LA regions with a thinner wall, whereas higher energy and longer contact time may be needed in regions with a thicker wall for complete transmural ablations.

6. Limitations

This study has several limitations. First, this study had a small sample size of patients with PeAF, although we used 25 preselected locations for each patient. Our findings need to be confirmed in a larger population. Second, LA size is dynamic as it changes with contraction and relaxation, which might affect the LAWT. The LAWT measured using cardiac CT before the ablation procedure may not correspond completely to the location on the electroanatomical mapping because the heart rate and volume status are often different between the time of pre-procedural cardiac CT and the time of electroanatomical mapping during the ablation procedure. Nonetheless, it has been reported that 3D electroanatomical mapping was well matched with CT images in patients undergoing catheter ablation for AF. Finally, the shapes and geometries of the LA may be different among patients owing to variabilities in the atrial remodeling process. To resolve this problem, the measurement points were not set at absolutely the same locations in all patients, but relative to the shape of the LA in each patient, as described in the Materials and Methods section. Additionally, we assessed parameters such that 10 points within 5 mm

of each reference point were measured, and calculated the average.

V. CONCLUSION

The LAWT has significant correlations with LA geometry and plays significant roles in human AF wave-dynamics, including electrical wave-break and rotors. In addition, there were significant regional differences in LAWT, LA geometry, and AF wave-dynamics, and their correlations.

REFERENCES

1. Allessie M, Ausma J, Schotten U. Electrical, contractile and structural remodeling during atrial fibrillation. Cardiovasc Res 2002;54:230-46.
2. Casaclang-Verzosa G, Gersh BJ, Tsang TS. Structural and functional remodeling of the left atrium: clinical and therapeutic implications for atrial fibrillation. J Am Coll Cardiol 2008;51:1-11.
3. Barbier P, Alioto G, Guazzi MD. Left atrial function and ventricular filling in hypertensive patients with paroxysmal atrial fibrillation. J Am Coll Cardiol 1994;24:165-70.
4. Dittrich HC, Pearce LA, Asinger RW, McBride R, Webel R, Zabalgoitia M, et al. Left atrial diameter in nonvalvular atrial fibrillation: An echocardiographic study. Stroke Prevention in Atrial Fibrillation Investigators. Am Heart J 1999;137:494-9.
5. Hansen BJ, Zhao J, Csepe TA, Moore BT, Li N, Jayne LA, et al. Atrial fibrillation driven by micro-anatomic intramural re-entry revealed by simultaneous sub-epicardial and sub-endocardial optical mapping in explanted human hearts. Eur Heart J 2015;36:2390-401.
6. Konings KT, Smeets JL, Penn OC, Wellens HJ, Allessie MA. Configuration of unipolar atrial electrograms during electrically induced atrial fibrillation in humans. Circulation 1997;95:1231-41.

7. Jalife J, Berenfeld O, Skanes A, Mandapati R. Mechanisms of atrial fibrillation: mother rotors or multiple daughter wavelets, or both? J Cardiovasc Electrophysiol 1998;9:S2-12.

8. Jalife J, Berenfeld O, Mansour M. Mother rotors and fibrillatory conduction: a mechanism of atrial fibrillation. Cardiovasc Res 2002;54:204-16.

9. Mandapati R, Skanes A, Chen J, Berenfeld O, Jalife J. Stable microreentrant sources as a mechanism of atrial fibrillation in the isolated sheep heart. Circulation 2000;101:194-9.

10. Chen J, Mandapati R, Berenfeld O, Skanes AC, Gray RA, Jalife J. Dynamics of wavelets and their role in atrial fibrillation in the isolated sheep heart. Cardiovasc Res 2000;48:220-32.

11. Kumagai K, Uno K, Khrestian C, Waldo AL. Single site radiofrequency catheter ablation of atrial fibrillation: studies guided by simultaneous multisite mapping in the canine sterile pericarditis model. J Am Coll Cardiol 2000;36:917-23.

12. Srichai MB, Barreto M, Lim RP, Donnino R, Babb JS, Jacobs JE. Prospective-triggered sequential dual-source end-systolic coronary CT angiography for patients with atrial fibrillation: a feasibility study. J Cardiovasc Comput Tomogr 2013;7:102-9.

13. Lin FY, Devereux RB, Roman MJ, Meng J, Jow VM, Jacobs A, et al. Cardiac chamber volumes, function, and mass as determined by

64-multidetector row computed tomography: mean values among healthy adults free of hypertension and obesity. JACC Cardiovasc Imaging 2008;1:782-6.

14. Wolf F, Ourednicek P, Loewe C, Richter B, Gossinger HD, Gwechenberger M, et al. Evaluation of left atrial function by multidetector computed tomography before left atrial radiofrequency-catheter ablation: comparison of a manual and automated 3D volume segmentation method. Eur J Radiol 2010;75:e141-6.

15. McAlpine WA. Heart and coronary arteries : an anatomical atlas for clinical diagnosis, radiological investigation, and surgical treatment. Berlin; New York: Springer-Verlag; 1975.

16. Nademanee K, McKenzie J, Kosar E, Schwab M, Sunsaneewitayakul B, Vasavakul T, et al. A new approach for catheter ablation of atrial fibrillation: mapping of the electrophysiologic substrate. J Am Coll Cardiol 2004;43:2044-53.

17. Roux JF, Gojraty S, Bala R, Liu CF, Dixit S, Hutchinson MD, et al. Effect of pulmonary vein isolation on the distribution of complex fractionated electrograms in humans. Heart Rhythm 2009;6:156-60.

18. Sanders P, Berenfeld O, Hocini M, Jais P, Vaidyanathan R, Hsu LF, et al. Spectral analysis identifies sites of high-frequency activity maintaining atrial fibrillation in humans. Circulation 2005;112:789-97.

19. Berenfeld O, Mandapati R, Dixit S, Skanes AC, Chen J, Mansour M, et al. Spatially distributed dominant excitation frequencies reveal hidden organization in atrial fibrillation in the Langendorff-perfused sheep heart. J Cardiovasc Electrophysiol 2000;11:869-79.

20. Skanes AC, Mandapati R, Berenfeld O, Davidenko JM, Jalife J. Spatiotemporal periodicity during atrial fibrillation in the isolated sheep heart. Circulation 1998;98:1236-48.

21. Ganesan AN, Kuklik P, Lau DH, Brooks AG, Baumert M, Lim WW, et al. Bipolar electrogram shannon entropy at sites of rotational activation: implications for ablation of atrial fibrillation. Circ Arrhythm Electrophysiol 2013;6:48-57.

22. Stokely EM, Wu SY. Surface Parameterization and Curvature Measurement of Arbitrary 3-D Objects - 5 Practical Methods. Ieee T Pattern Anal 1992;14:833-40.

23. Nunes MC, Handschumacher MD, Levine RA, Barbosa MM, Carvalho VT, Esteves WA, et al. Role of LA shape in predicting embolic cerebrovascular events in mitral stenosis: mechanistic insights from 3D echocardiography. JACC Cardiovasc Imaging 2014;7:453-61.

24. Bisbal F, Gomez-Pulido F, Cabanas-Grandio P, Akoum N, Calvo M, Andreu Beng D, et al. Left Atrial Geometry Improves Risk Prediction of Thromboembolic Events In Patients with Atrial Fibrillation. J Cardiovasc Electrophysiol 2016;27:804-10.

25. Kurotobi T, Iwakura K, Inoue K, Kimura R, Toyoshima Y, Ito N, et al. The significance of the shape of the left atrial roof as a novel index for determining the electrophysiological and structural characteristics in patients with atrial fibrillation. Europace 2011;13:803-8.

26. Bisbal F, Guiu E, Calvo N, Marin D, Berruezo A, Arbelo E, et al. Left atrial sphericity: a new method to assess atrial remodeling. Impact on the outcome of atrial fibrillation ablation. J Cardiovasc Electrophysiol 2013;24:752-9.

27. Inoue YY, Alissa A, Khurram IM, Fukumoto K, Habibi M, Venkatesh BA, et al. Quantitative tissue-tracking cardiac magnetic resonance (CMR) of left atrial deformation and the risk of stroke in patients with atrial fibrillation. J Am Heart Assoc 2015;4.

28. Watson T, Shantsila E, Lip GY. Mechanisms of thrombogenesis in atrial fibrillation: Virchow's triad revisited. Lancet 2009;373:155-66.

29. Takahashi K, Okumura Y, Watanabe I, Nagashima K, Sonoda K, Sasaki N, et al. Relation Between Left Atrial Wall Thickness in Patients with Atrial Fibrillation and Intracardiac Electrogram Characteristics and ATP-Provoked Dormant Pulmonary Vein Conduction. J Cardiovasc Electrophysiol 2015;26:597-605.

30. Beinart R, Abbara S, Blum A, Ferencik M, Heist K, Ruskin J, et al. Left atrial wall thickness variability measured by CT scans in patients

undergoing pulmonary vein isolation. J Cardiovasc Electrophysiol 2011;22:1232-6.

31. Park J, Joung B, Uhm JS, Shim CY, Hwang C, Lee MH, et al. High left atrial pressures are associated with advanced electroanatomical remodeling of left atrium and independent predictors for clinical recurrence of atrial fibrillation after catheter ablation. Heart Rhythm 2014;11:953-60.

32. Nakamura K, Funabashi N, Uehara M, Ueda M, Murayama T, Takaoka H, et al. Left atrial wall thickness in paroxysmal atrial fibrillation by multislice-CT is initial marker of structural remodeling and predictor of transition from paroxysmal to chronic form. Int J Cardiol 2011;148:139-47.

33. Kalifa J, Tanaka K, Zaitsev AV, Warren M, Vaidyanathan R, Auerbach D, et al. Mechanisms of wave fractionation at boundaries of high-frequency excitation in the posterior left atrium of the isolated sheep heart during atrial fibrillation. Circulation 2006;113:626-33.

34. Ciaccio EJ, Biviano AB, Whang W, Gambhir A, Garan H. Spectral profiles of complex fractionated atrial electrograms are different in longstanding and acute onset atrial fibrillation atrial electrogram spectra. J Cardiovasc Electrophysiol 2012;23:971-9.

35. Morillo CA, Klein GJ, Jones DL, Guiraudon CM. Chronic rapid atrial pacing. Structural, functional, and electrophysiological characteristics

of a new model of sustained atrial fibrillation. Circulation 1995;91:1588-95.

36. Ausma J, Wijffels M, Thone F, Wouters L, Allessie M, Borgers M. Structural changes of atrial myocardium due to sustained atrial fibrillation in the goat. Circulation 1997;96:3157-63.

37. Imada M, Funabashi N, Asano M, Uehara M, Ueda M, Komuro I. Anatomical remodeling of left atria in subjects with chronic and paroxysmal atrial fibrillation evaluated by multislice computed tomography. Int J Cardiol 2007;119:384-8.

38. Park JH, Park SW, Kim JY, Kim SK, Jeoung B, Lee MH, et al. Characteristics of complex fractionated atrial electrogram in the electroanatomically remodeled left atrium of patients with atrial fibrillation. Circ J 2010;74:1557-63.

39. Dickfeld T, Tian J, Ahmad G, Jimenez A, Turgeman A, Kuk R, et al. MRI-Guided ventricular tachycardia ablation: integration of late gadolinium-enhanced 3D scar in patients with implantable cardioverter-defibrillators. Circ Arrhythm Electrophysiol 2011;4:172-84.

40. Hwang M, Song JS, Lee YS, Li C, Shim EB, Pak HN. Electrophysiological Rotor Ablation in In-Silico Modeling of Atrial Fibrillation: Comparisons with Dominant Frequency, Shannon Entropy, and Phase Singularity. PloS one 2016;11:e0149695.

41. Li C, Lim B, Hwang M, Song JS, Lee YS, Joung B, et al. The Spatiotemporal Stability of Dominant Frequency Sites in In-Silico Modeling of 3-Dimensional Left Atrial Mapping of Atrial Fibrillation. PloS one 2016;11:e0160017.

42. Hwang M, Kwon SS, Wi J, Park M, Lee HS, Park JS, et al. Virtual ablation for atrial fibrillation in personalized in-silico three-dimensional left atrial modeling: comparison with clinical catheter ablation. Prog Biophys Mol Biol 2014;116:40-7.

43. Hwang M, Park J, Lee YS, Park JH, Choi SH, Shim EB, et al. Fibrillation number based on wavelength and critical mass in patients who underwent radiofrequency catheter ablation for atrial fibrillation. IEEE Trans Biomed Eng. 2015;62:673-9.

ABSTRACT (IN KOREAN)

심방세동 파동역학에 있어 심방 벽두께의 역할

<지도교수 박희남>

연세대학교 대학원 의학과

위진

서론: 심방세동의 진행은 좌심방의 구조 변화를 야기하며 그 자체로도 심방세동을 유발한다. 이는 곧 좌심방 구조와 심방세동 파동역학 상호간에 영향을 주고 받는다는 것을 의미한다. 본 연구에서는 좌심방 벽두께와 심방 기하구조, 심방세동 파동역학의 상호관련성을 분석하였다.

대상 및 방법: 심방세동 카테터 절제술을 시행 받은 27명의 심방세동 환자를 대상으로 하였다 (지속성 15명, 발작성 12명). 시술 전 시행한 심장 컴퓨터 단층촬영 영상을 이용해 좌심방 내 25개 위치에서 벽두께 및 평탄도 (bumpiness) 를 측정하였다. 또한 각

환자로부터 시술 중 직접 획득된 심방세동 electrogram을 특수 고안된 소프트웨어를 사용하여 complex fractionated atrial electrogram (CFAE), dominant frequency (DF), Shannon entropy (ShEn) 와 같은 파동역학 변수들을 계산하였다.

결과: 1. 좌심방 벽두께는 환자, 측정부위, 심방세동의 종류에 따라 다양하게 측정되었다. 평균 벽두께는 2.1 ± 0.6 mm 였으며 각 지역별로 1.9 mm 에서 3.1 mm 까지 다양성을 보였다. 2. 지속성 심방세동 환자의 벽두께는 좌심방의 부피가 증가할수록 감소하는 음의 상관관계를 나타내었으나 ($r = -0.565$, $p = 0.028$) 발작성 심방세동의 경우 유의한 상관관계를 보이지 않았다. 3. 심방 벽두께는 평탄도 ($r = 0.272$, $p < 0.001$), ShEn ($r = 0.233$, $p < 0.001$) 와 유의한 양의 상관관계를 나타내었고, CFAE 순환주기 (CFAE-CL) 와는 음의 상관관계를 나타내었다 ($r = -0.107$, $p = 0.038$). 4. 파동역학 변수들과 심방 벽두께간의 다중회귀분석에서 DF는 심방 벽두께 ($\beta = -0.29$, $p < 0.001$), ShEn ($\beta = 0.74$, $p < 0.001$) 와 유의한 관련성을 보여 주었다. ShEn 는 심방 벽두께 ($\beta = 0.19$, $p < 0.001$), DF ($\beta = 0.14$, $p < 0.001$), CFAE-CL ($\beta = -0.01$, $p < 0.001$) 와 유의한 상관관계를 나타내었다. CFAE-CL 역시 심방 벽두께 ($\beta = 7.49$, $p = 0.032$), ShEn ($\beta = -74.00$, $p < 0.001$) 와 유의한 관련성을 보여 주었다.

결론: 좌심방 벽두께는 지역별, 심방세동 종류에 따라 다르게 변화하며, 심방세동 파동역학, 전기적 wave-break, rotors 등과 밀접한 관련성을 가진다는 것을 확인하였다.

핵심되는 말: 심방세동, 벽두께, 평탄도, 파동역학